Myosin Motor Domain Lever Arm Rotation Is Coupled to ATP Hydrolysis†

Stefan Highsmith,*,‡ Katherine Polosukhina,‡ and Don Eden§

Department of Biochemistry, University of the Pacific, School of Dentistry, San Francisco, California 94115-2399, and Department of Chemistry and Biochemistry, San Francisco State University, San Francisco, California 94132

Received May 22, 2000; Revised Manuscript Received August 1, 2000

ABSTRACT: We have investigated coupling of lever arm rotation to the ATP binding and hydrolysis steps for the myosin motor domain. In several current hypotheses of the mechanism of force production by muscle, the primary mechanical feature is the rotation of a lever arm that is a subdomain of the myosin motor domain. In these models, the lever arm rotates while the myosin motor domain is free, and then reverses the rotation to produce force while it is bound to actin. These mechanical steps are coupled to steps in the ATP hydrolysis cycle. Our hypothesis is that ATP hydrolysis induces lever arm rotation to produce a more compact motor domain that has stored mechanical energy. Our approach is to use transient electric birefringence techniques to measure changes in hydrodynamic size that result from lever arm rotation when various ligands are bound to isolated skeletal muscle myosin motor domain in solution. Results for ATP and CTP, which do support force production by muscle fibers, are compared to those of ATPγS and GTP, which do not. Measurements are also made of conformational changes when the motor domain is bound to NDP's and PP_i in the absence and presence of the phosphate analogue orthovanadate, to determine the roles the nucleoside moieties of the nucleotides have on lever arm rotation. The results indicate that for the substrates investigated, rotation does not occur upon substrate binding, but is coupled to the NTP hydrolysis step. The data are consistent with a model in which only substrates that produce a motor domain−NDP−P_i complex as the steady-state intermediate make the motor domain more compact, and only those substrates support force production.

Skeletal muscle myosin has two motor domains that are attached to a coiled-coil domain by a flexible linkage. Each motor domain comprises a catalytic subdomain and a regulatory subdomain. The regulatory subdomain, also referred to as a lever arm, can rotate. Lever arm rotation while the catalytic subdomain is bound to actin may generate force during muscle contraction (*1*, *2*). For any mechanism of force production, it is important to know how the mechanical cycle is coupled to the catalytic cycle of ATP hydrolysis. During a catalytic cycle, a motor domain dissociates from actin, hydrolyzes ATP, and rebinds actin (*3*). At the scale of protein subdomain rearrangements, most rotating lever arm models of force production have the lever arm rotate while the motor domain is free, and then reverse the rotation when it is bound to actin.

In a simplified low-resolution scheme (Figure 1), mechanochemical coupling occurs explicitly in two reactions. In step 3, lever arm rotation is coupled to ATP hydrolysis, storing mechanical energy in a more compact motor domain structure. In step 5, some form of reverse rotation is coupled to product release, liberating the stored mechanical energy. There is some evidence to support the coupling of the specific mechanical changes to the steps of the hydrolytic cycle as shown. Crystal structures of isolated motor domain−nucleotide complexes indicate that it is possible for the lever arm to assume different orientations (*4*−*6*). In solution, the structures of M·MgADP·P_i and of the analogues M·MgADP·V_i[1] and M·MgADP·AlF_4 have smaller hydrodynamic size or radii of gyration compared to M·MgADP (*7*−*10*), consistent with ATP binding and/or hydrolysis inducing lever arm rotation to a more compact structure. Kinetic data indicate force production is coupled to P_i release (*11*, *12*), consistent with mechanical coupling to step 5 in Figure 1. Nucleotide-dependent lever arm rotation for myosin motor domains bound to actin has been observed by electron microscopy (*13*) and from orientation reporter molecules attached to lever arms (*14*, *15*). However, the data are mostly indirect and were obtained using fibers and proteins from various types of muscles; many questions remain as to whether the scheme shown in Figure 1 is correct (*16*).

In the work reported here, we address the chemomechanics of step 3 (Figure 1). Specifically, is lever arm rotation of the actin-free motor domain coupled to ATP hydrolysis, and is lever arm rotation by the free motor domain necessary for force production? Our primary approach is to use transient electric birefringence techniques to measure changes in hydrodynamic size that result from lever arm rotation of the myosin motor domain in solution (*1*, *8*). The results for ATP are compared to those of ATP analogues that do or do not

† Supported by NIH Grants AR42895, GM52588, and RR11805.

* Correspondence should be addressed to this author at the Department of Biochemistry, University of the Pacific, School of Dentistry, San Francisco, CA 94115-2399. E-mail: shighsmith@uop.edu.

‡ University of the Pacific, School of Dentistry.

§ San Francisco State University.

[1] Abbreviations: S1, myosin subfragment 1; TEB, transient electric birefringence; τ_{20}, rotational decay times adjusted to 20 °C; Mops, 3-(*N*-morpholino)propanesulfonic acid; NTP, nucleoside triphosphate; NDP, nucleoside diphosphate; ATPγS, adenosine 5′-γ-thiotriphosphate; PP_i, pyrophosphate; V_i, orthovanadate; OAc, acetate.

10.1021/bi001146d CCC: $19.00
Published on Web 09/14/2000

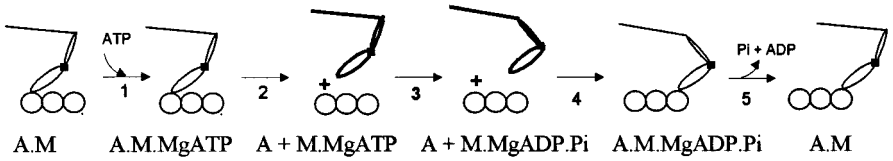

FIGURE 1: Actin−myosin−ATP mechanical and hydrolytic cycles. A is actin. M is a myosin motor domain, or S1 moiety. Step 1: MgATP binds to the A·M complex. Step 2: M·MgATP dissociates from A. Step 3: Hydrolysis of ATP by actin-free M·MgATP induces the rotation of the lever arm, and creates a more compact motor domain with stored mechanical energy. The coupling of mechanical and chemical cycles in step 3 is investigated in the present work. Step 4: M·MgADP·P_i binds to actin. Step 5: Force is produced, and the ATP hydrolysis products dissociate and the lever arm rotation reverses.

support force production by muscle fibers. Advantage is taken of previous results of others indicating that ATP and CTP support force production, while GTP and ATPγS do not (*17*, *18*). To determine what roles the nucleosides have on lever arm rotation, measurements were also made of conformational changes when the motor domain is bound to NDP's and PP_i in the absence and presence of the phosphate analogue orthovanadate. The results presented below indicate that lever arm rotation is coupled to substrate hydrolysis, as opposed to binding, and that lever arm rotation by the free motor domain creates stored mechanical energy that is required for force production.

MATERIALS AND METHODS

Proteins and Chemicals. Myosin subfragment 1 (S1) was produced from skeletal muscle myosin by proteolysis using papain (*19*). The crude S1 was loaded on a Sephacryl 400 column and eluted with 50 mM imidazole (pH 7.0), 1 mM $MgCl_2$. The center fractions of the single peak were collected and loaded on a Whatman DE-52 ion change column, 100 mL of 50 mM imidazole, 1 mM $MgCl_2$ buffer was passed through the column, and crude S1 was eluted with 0.12 M NaCl in the column buffer. The partially purified S1 was dialyzed to 10 mM Mops, 2 mM $MgCl_2$, loaded on a Pharmacia Mono Q 5/5 column, and eluted with a 0−0.50 M NaCl gradient. The major peak was collected, loaded on a Superdex 200 column, and eluted with TEB buffer [5 mM Mops (pH 7.0), 1 mM KOAc, 0.6 mM $MgOAc_2$]. The center of the single symmetrical peak was collected and used for the measurements.

Commercial ATPγS was purified by ion exchange chromatography (*20*). Purity of the ATPγS sample was monitored by reverse-phase HPLC using a C18 Ultrasphere 1B column eluted isocratically with 25% acetonitrile in 30 mM KH_2PO_4, 10 mM TBAP (tetrabutylammonium phosphate), pH 7.0. The purified material was 95% ATPγS, and was stable for up to 2 weeks, when stored at −20 °C. ATP, CTP, GTP, and PP_i were purchased from Sigma and used without further purification. Orthovanadate was prepared as described previously (*21*) and used immediately.

Activity Assays. MgNTPase activities were measured at 25 °C for 1 μM S1 in TEB buffer with 0.50 mM NTP present. The production of orthophosphate was determined using a Malachite green method (*22*).

Phosphate Analogue Complex Formation. Formation of S1·MgNDP·V_i complexes in TEB buffer with 0.50 mM NDP and 0.50 mM V_i was determined by the loss of MgNTPase activity. For complexes of S1 in TEB buffer containing 0.50 mM PP_i and 0.50 mM V_i, the amount of bound orthovanadate was measured directly. A solution of S1·$MgPP_i$·V_i was centrifuged at 20000*g* to transfer 10% of the total volume through a 30 000 Da cutoff filter. Bound V_i was the difference between the total vanadate in the filtered and unfiltered portions, using a vanadate assay (*24*). Parallel measurements of S1·MgADP·V_i were used as a standard. This is not a true equilibrium method, and unlike the activity assays, it requires higher [S1] than used in the TEB measurements.

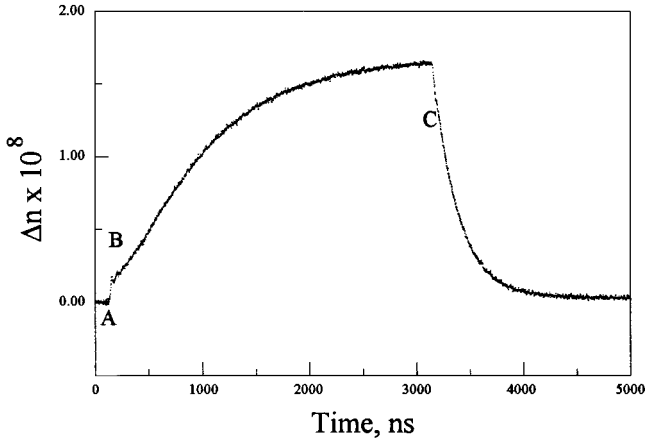

FIGURE 2: Transient electric birefringence signal. The birefringence, Δn, is shown for 1.0 μM S1 in 5.0 mM Mops (pH 7.0), 1.0 mM KOAc, 0.60 mM $MgOAc_2$, 0.50 mM GDP, 0.50 mM P_i at 22 °C in response to the application of a 3.0 μs 2860 V/cm pulse. The very fast increase at the start of the electric field pulse, A, is due to the alignment of water by the field. The sigmoidal shape in the early part of the signal increase, B, may be due to S1·MgGDP rotation about its long axis (see text). The terminal rotational decay time, τ, was obtained by fitting the data beginning at 70 ns after the electric field was removed, C. For the data shown, $\tau = 248.9$ ns. Several measurements were averaged and converted to τ_{20} (Table 2).

TEB Measurements. The instrument, equipped with a 3 cm path length cell, has been described (*25*). All samples were 1 μM S1 in TEB buffer with 0.50 mM nucleotide or PP_i, and 0.50 mM P_i or V_i, as indicated. For NTP's, data collection was finished before 50% of the NTP was hydrolyzed. The birefringence changes of a solution of 1 μM S1·MgGDP, in response to a 3 μs 2860 V/cm square pulse (Figure 2), are typical. The signal, Δn, almost reaches its steady-state value, making its decay rate independent of field strength or duration (*26*). The decay of the signal after the field is removed is analyzed using the program DISCRETE (*27*) to obtain decay times, τ, that have contributions from the end-over-end rotation and any segmental motions of the S1−nucleotide complex. The terminal decay time is dominated by the end-over-end rotation, and is the one that has been used to estimate the length of the hydrated complex (*26*). TEB decay times are sensitive to length changes. The decay times can be analyzed to obtain estimates of myosin motor domain lever arm rotation that are consistent with

Table 1: S1·MgNDP·V_i Complex Formation[a]

ligand	NTPase activity, s^{-1}	NDP−vanadate complex, %
ATP	0.071 ± 0.006	95 ± 6
ATPγS	0.072 ± 0.006	−
CTP	0.040 ± 0.003	84 ± 7
GTP	0.093 ± 0.007	46 ± 8
PP_i	0	7 ± 5

[a] NTPase activities at 25 °C in 5 mM Mops (pH 7.0), 1 mM KOAc, 0.60 mM $MgOAc_2$, and 0.50 mM NTP. NDP-vanadate complex formation is estimated from the loss of NTPase activity in the presence of 0.50 mM vanadate and 0.50 mM ADP, CDP, or GDP, in the same TEB buffer. Vanadate complex formation in the presence of PP_i was estimated from the amount of bound vanadate in the presence of 0.50 mM PP_i. Experimental uncertainties are standard errors for five or more measurements.

Table 2: S1−Steady-State and −Product Complex Rotational Decay Times, τ_{20} (ns)[a]

substrate	steady state	product	force[b]
ATP	241.5 ± 0.9	252.9 ± 1.4	100
CTP	241.0 ± 3.1	250.5 ± 1.7	80−90
GTP	251.1 ± 1.3	248.9 ± 2.2	10
ATPγS	252.0 ± 2.1	252.9 ± 1.4	∼0

[a] Terminal decay times in ns of a birefringence signal, after an aligning electric field was removed, were measured at 22 °C (see Figure 2) and adjusted to 20 °C decay times, τ_{20}. Values are averages of at least three measurements. Experimental uncertainties are standard errors. When no ligand is present, τ_{20} is 248.0 ns. [b]Normalized force values are for skinned single fibers from rabbit psoas muscle (*17*, *18*). Only the force-producing substrates form steady-state intermediates that have reduced τ_{20} values.

those obtained by X-ray crystallography (*4*, *5*) and by X-ray or neutron scattering from S1 complexes in solution (*9*, *10*).

The data have an interesting feature in the rise of the birefringence signal. Immediately after the rapid increase in birefringence due to the alignment of water molecules (A in Figure 2), there is a contribution from a rapid birefringence decrease (B in Figure 2). Combined with the slower and much larger positive birefringence increase due to the end-over-end alignment of S1, the negative contribution gives the early portion of the curve a sigmoidal shape. This feature is present in all S1 data, although it is clearer in data collected with the improved instrument used here. The negative contribution may be due to rapid rotation of S1's large permanent electric dipole moment about its major axis, assuming that the electric dipole axis is not precisely parallel to the major axis of the molecule, a hypothesis that can be investigated in future studies. In any event, there is a counterpart of this rapid negative birefringence in the decay of the signal. It is not as evident in the decay of the signal, because for S1 the rate of decay is 3 times as large as that of the rise (*26*). However, because it is the terminal decay time that is due to the electric field-free end-over-end rotation of the S1 complex, it is important to exclude contributions from the rapid negative contribution, whatever its source. To ensure this, the decay times were determined by analyzing the data for an interval of 700 ns beginning 70 ns after the field was removed (C in Figure 2). Decay times were measured at ∼22 °C and converted to 20 °C decay times, τ_{20}, using the equation: $\tau_{20} = \tau_T(\eta_{20}/\eta_T)(T/293.15)$, where τ_T is the decay time measured at T, and η is the viscosity of water (Tables 2 and 3).

Fluorescence Measurements. Steady-state intrinsic tryptophan fluorescence intensities of S1−nucleotide complexes at 25 °C in TEB buffer were measured using a Hitachi-Perkin-Elmer MPF-44B fluorospectrophotometer. The signal for 1 μM S1 in 5 mM Mops (pH 7.0), 1 mM KOAc, 0.60 mM $MgOAc_2$ was set to 100, and NDP or NTP was added to obtain 0.5 mM. Intensities were corrected for dilution. Irradiation was at 300 nm, and the intensity of light emitted at 337 nm was measured.

RESULTS

S1 Complexes. Activities and vanadate complex stabilities were characterized in the buffer used for the TEB measurements (Table 1). The NTPase activities at 25 °C are within the ranges reported for myosin and S1 activities in higher ionic strength buffers (*28*−*30*). Pyrophosphate is not a substrate for myosin. Loss of NTPase activity was used to estimate what percentage of the S1 formed a complex with NDP and vanadate. S1·MgADP·V_i and S1·MgCDP·V_i approach stoichiometric inactivation, when incubated overnight at 0 °C and then warmed to 25 °C for activity measurements. When the loss of activity at 25 °C was monitored over time, inactivation was complete within 40 min after adding the orthovanadate (data not shown). The S1·MgGDP·V_i complex is less stable, accounting for less than 50% of the S1 present. Increasing the incubation period (to 48 h), the [vanadate], the [GDP], or the temperature (to 25 °C) had little effect. The S1·$MgPP_i$·V_i complex is much less stable (Table 1).

TEB Measurements. The terminal decay times, τ_{20}, of the birefringence signals for S1 in the presence of four substrates are shown in Table 2. The conditions are described under Materials and Methods. The results for the ATP are consistent with previous studies at lower temperature (*25*). The steady-state intermediate complex formed by ATP is more compact than the one formed by ADP. The results for CTP and CDP are close to those for the adenine pair, indicating that the steady-state intermediate S1·MgCDP·P_i is more compact than the product complex S1·MgCDP. Results for the guanine pair, on the other hand, indicate that there is no diminution in hydrodynamic size for the complex formed by GTP, as compared to S1·MgGDP. The results for the analogue of unhydrolyzed ATP, ATPγS, are similar to those for GTP. The hydrodynamic size of the S1·MgATPγS complex is near that of S1·MgADP or of S1 without a ligand. This is an important result, indicating that ATP binding does not make S1 more compact. The normalized force produced by skinned skeletal muscle fibers (Table 2) when the substrates are ATP, CTP, GTP (*17*), and ATPγS (*18*) indicates that the formation of a compact steady-state intermediate correlates strongly with force production.

The effect of othovanadate, V_i, binding on τ_{20} for S1 nucleotide diphosphate and pyrophosphate complexes was determined. The conditions were identical to those used for the substrate measurements. For S1·MgADP and S1·MgCDP, τ_{20} is reduced when V_i binds, indicating that the vanadate complex is more compact (Table 3). V_i is a P_i analogue, and the formation of a more compact complex is consistent with the ATP and CTP steady-state results (Table 2), and with the nearly complete inhibition of ATPase and CTPase activities (Table 1). The small decrease in hydrodynamic size for S1 in the presence of PP_i and V_i (Table 3) is consistent with the small amount of V_i bound to S1·$MgPP_i$

Table 3: S1 Diphosphate and Vanadate Complex Rotational Decay Times, τ_{20} (ns)[a]

ligand	$-V_i$	$+V_i$
ADP	252.9 ± 1.4	227.3 ± 1.5
CDP	250.5 ± 1.7	232.2 ± 2.1
GDP	248.9 ± 2.2	236.0 ± 2.2
PP_i	247.1 ± 1.3	244.0 ± 1.0

[a] Terminal decay times in ns of a birefringence signal, after an aligning electric field was removed, were measured at 22 °C (see Figure 2) and adjusted to 20 °C decay times, τ_{20}. Values are averages of at least three measurements. Experimental uncertainties are standard errors. When no ligand is present, τ_{20} is 248.0 ns.

Table 4: S1−Nucleotide Complex Intrinsic Fluorescence Intensity Changes[a]

base, N	MgNDP	MgNTP	increase, %
adenine	105.7 ± 1.1	113.5 ± 1.3	7.8 ± 1.5
cytosine	100.5 ± 0.8	107.0 ± 0.6	6.5 ± 1.1
guanine	86.8 ± 2.6	86.6 ± 2.1	0.2 ± 3.1

[a] The steady-state fluorescence intensity of S1 with no ligand was set to 100. Values are averages of at least four measurements. Experimental uncertainties are standard errors.

(Table 1). The complex obtained with GDP + V_i is more compact than S1·MgGDP, but not to the degree observed for ADP and CDP (Table 3). This is consistent with only partial formation of S1·MgGDP·V_i compared to the adenine and cytosine complexes. The incomplete loss of GTPase activity when S1 is incubated with GDP and V_i (see above) also suggests that S1·MgGDP·V_i is not as stable as its ADP or CDP counterparts (Table 1).

S1 Intrinsic Fluorescence Intensity. S1 steady-state intrinsic fluorescence intensity is a sensitive indicator of conformational changes induced by ligand binding, temperature, and buffer conditions. The atomic level structural changes that cause the fluorescence intensity changes are not understood, but when S1 reacts with ATP there is a 10−30% increase over the value of S1 alone (*31*), depending on the excitation and emission wavelengths. ADP induces a smaller increase. Steady-state fluorescence intensities were measured at 25 °C for S1 in the presence of NTP's and NDP's for conditions identical those used for the TEB measurements. The changes in intensity were base-dependent. For the NDP's, compared to S1 alone, GDP caused a 13% decrease, while CDP and ADP caused 0 and 6% increases, respectively (Table 4). Comparing the NDP's to the corresponding NTP's, GTP induced no additional change, while CTP and ATP induce 7% increases over their NDP counterparts.

The large decrease observed for GDP and GTP is not unique; cross-linking Cys-967 to Cys-707 in the absence of nucleotide induces a 28% decrease (*32*), indicative of the sensitivity of S1 tryptophan fluorescence intensity to ligand binding and to other conformational changes. More interestingly, the substrates that support force production by muscle fibers, and induce the formation of compact steady-state intermediates (Table 2), have similar changes for S1 in the presence of NTP compared to NDP (Table 4). This result suggests that when the differences due to cytosine and adenine are accounted for, the internal S1 conformational changes for the NTP to NDP transitions are similar for CTP and ATP.

DISCUSSION

Two major conclusions can be drawn from the results presented here. First, substrate hydrolysis to form a steady-state intermediate S1·MgNDP·P_i is coupled to lever arm rotation, which creates a more compact motor domain that has stored mechanical energy. Second, a motor domain steady-state intermediate with the lever arm rotated is required for force generation. The substrates ATP and CTP, which support force generation by muscle fibers (*17*), also produce more compact motor domain steady-state intermediates in solution (Table 2). For these force-producing substrates, the steady-state intermediates have the hydrolysis products NDP and P_i bound in the active site (*28, 33*). In contrast, the substrates ATPγS and GTP, which do not support force (*17, 18*), do not produce compact steady-state intermediates (Table 2). The steady-state intermediates for these nonproductive substrates have unhydrolyzed MgATPγS or MgGTP in the active site (*30, 34*). The structural data reported here for ATP, CTP, GTP, and ATPγS complement the pioneering physiological (*17, 18*) and kinetic (*28, 33*) studies of these substrates using muscle fibers, and support strongly the validity of step 3 as depicted in Figure 1.

Complexes of S1 and nucleoside diphosphates, which also have V_i bound, are more stable than the steady-state intermediates that have P_i bound (*24, 35*). The TEB data indicate that S1·MgNDP·V_i complexes are more compact than their P_i counterparts for ADP, CDP, and GDP (Table 3). Steady-state intermediates comprise the equilibrium S1·MgNTP ↔ S1·MgNDP·P_i (*33*), which is probably driven to the right when V_i replaces P_i. The smaller τ_{20} observed for S1·MgNDP in the presence of V_i would then be due to more of S1 being in the S1·MgNDP·P_i conformation, which is more compact than the S1·MgNTP conformation. The alternative, that the S1·MgNDP·V_i complex has the lever arm rotated to a greater degree than the S1·MgNDP·P_i complex, cannot be excluded.

It is interesting that both the GTPase activity loss (Table 1) and the decrease in τ_{20} (Table 3) indicate that V_i binds to form S1·MgGDP·V_i, but the τ_{20} data indicate that the GTP steady-state intermediate is not more compact (Table 2). Part of the explanation for this apparent discrepancy is that the steady-state intermediate for GTP hydrolysis is S1·MgGTP not S1·MgGDP·P_i (*34*). In addition, the data indicate S1·MgGDP·V_i complex is not as stable as those formed with ADP or CDP, which is consistent with the reported lack of increase in melting temperature for S1·MgGDP in the presence of V_i (*35*). There is no discrepancy if the free energy of V_i binding to S1·MgGDP is able to overcome partially the destabilizing contribution that guanine has on the formation of S1·MgGDP·P_i. What is particularly relevant here is that when the complex is formed, even if forced by V_i binding energy, the structure becomes more compact (Table 3). This result suggests that occupancy of the γ-phosphoryl binding sub-site by phosphate or by a close structural and electronic analogue of phosphate is critical for formation of a more compact S1 structure.

The PP_i data (Tables 1 and 3) demonstrate that although a base such as guanine can destabilize the formation of S1·MgNDP·P_i or S1·MgNDP·V_i, interaction of the base binding and the γ-phosphoryl binding sub-sites of the ATP binding site is required for strong V_i binding. In the absence of other

ligands, V_i binding to S1 is weak (*24*). The direct measurement of V_i binding to S1·$MgPP_i$ (Table 1) and the insignificant reduction in τ_{20} of S1·$MgPP_i$ in the presence of V_i (Table 3) indicate V_i binding to S1·$MgPP_i$ is also weak. A true nucleoside is not required, V_i binds to nonnucleoside diphosphate−S1 complexes (*36*), but the nucleoside site needs to be occupied.

The fluorescence intensity changes for nucleotide binding are sensitive to ligand occupancy of the base binding and phosphoryl binding sub-sites of the ATP site (Table 4), as has been reported in many earlier studies. Interpretation of myosin intrinsic fluorescence intensity changes is rarely unambiguous, although several recent reports indicate that Trp-510 is responsible for the ATP-induced fluorescence intensity increase (*38*−*41*). It is worth noting that the changes (∼−7%) observed for the S1·MgADP·P_i to S1·MgADP and the S1·MgCDP·P_i to S1·MgCDP transitions are equal within experimental error (Table 4). Bound to actin, this transition is the force-producing step (*11*, *12*). S1·MgADP·P_i and S1·MgCDP·P_i are the steady-state intermediates that are more compact, and that support contraction. The equal fluorescence intensity changes for P_i loss are consistent with equal internal conformational changes for the force-producing step 5 in Figure 1.

TEB was used to measure the hydrodynamic sizes of the S1 complexes. Previous studies have shown that the decreases in hydrodynamic size are consistent with rotation of an S1 segment comparable to its lever arm (*1*, *25*). Other S1 structural changes, such as opening or closing of the actin binding cleft (*4*), cannot be excluded as possible contributors to the observed changes in hydrodynamic size. The interpretation that is most consistent with the known S1 structural changes is that the more compact S1 structures have the lever arm rotated to an angle smaller than that of less compact structures. The crystal structures of elongated (*4*) and compact (*5*) myosin motor domains may provide atom level details for the lever arm rotation to store mechanical energy, which occurs during or after substrate hydrolysis in the mechanical and hydrolysis cycle (Figure 1).

It is noteworthy that the standard free energies of hydrolyses of the three NTP's are nearly equal. The GDP vanadate data, both the inhibition of GTPase activity and the compact structure observed for GDP·V_i, suggest that when GTP is hydrolyzed, a compact S1·MgGDP·P_i may be formed, although it is unstable and short-lived. This is likely to be case for ATPγS hydrolysis as well. Thus, it appears that the mechanical coupling that underlies energy transduction has a crucial kinetic component. S1·NDP·P_i must persist long enough to interact with actin. In the case of the reduced force observed when CaATP is the substrate (*37*), it is clear that compact S1·CaADP·P_i and S1·CaADP·V_i structures are formed. But it appears that compared to S1·MgADP·P_i, a larger fraction of the S1·CaADP·P_i formed dissociates P_i before the complex can bind actin. For ATPγS and GTP, the S1·MgNDP·P_i, if formed, must be even less stable, and less likely to bind to an actin.

In summary, the results presented here, along with earlier data on force generation, suggest that substrate hydrolysis-driven rotation of the myosin motor domain lever arm to produce a compact structure that has stored mechanical energy must occur before binding to actin, in order for force to be produced.

REFERENCES

1. Highsmith, S., and Eden, D. (1990) *Biochemistry 29*, 4087−4093.
2. Rayment, I., Holden, H. M., Whittaker, M., Yohn, C. B., Lorenz, M., Holmes, K. C., and Milligan, R. A. (1993) *Science 261*, 58−65.
3. Lymn, R. W., and Taylor, E. W. (1971) *Biochemistry 10*, 4617−4624.
4. Rayment, I., Rypniewski, W. R., Schmidt-Base, K., Smith, R., Tomchick, D. R., Benning, M. M., Winkelmann, D. A., Wesenberg, G., and Holden, H. M. (1993) *Science 261*, 50−58.
5. Dominguez, R., Freyzon, Y., Trybus, K. M., and Cohen, C. (1998) *Cell 94*, 559−571.
6. Houdusse, A., Kalbokis, V. N., Himmel, D., Szentgyorgyi, A. G., and Cohen, C. (1999) *Cell 97*, 459−470.
7. Aguirre, R., Gonsoulin, F., and Cheung, H. C. (1986) *Biochemistry 25*, 7−6835.
8. Highsmith, S., and Eden, D. (1993) *Biochemistry 32*, 2455−2458.
9. Wakabayashi, K., Tokunaga, M., Kohno, I., Sugimoto, Y., Hamanaka, T., Takezawa, Y., Wakabayashi, T., and Amemiya, Y. (1992) *Science 258*, 443−447.
10. Mendelson, R. A., Schneider, D. K., and Stone, D. B. (1996) *J. Mol. Biol. 256*, 1−7.
11. Johnson, K. A., and Taylor, E. W. (1978) *Biochemistry 17*, 3432−3442.
12. Webb, M. R., Hibberd, M. G., Goldman, Y. E., and Trentham, D. R. (1986) *J. Biol. Chem. 261*, 15557−15564.
13. Whittaker, M., Wilson-Kubalek, E. M., Smith, J. E., Faust, L., Milligan, R. A., and Sweeney, H. L. (1995) *Nature 378*, 748−751.
14. Gollub, J., Cremo, C. R., and Cooke, R. (1996) *Nat. Struct. Biol. 3*, 796−802.
15. Hopkins, S. C., Sabido-David, C., Corrie, J. E. T., Irving, M., and Goldman, Y. E. (1998) *Biophys. J. 74*, 3093−3110.
16. Highsmith, S. (1999) *Biochemistry 38*, 9791−9797.
17. Pate, E., Franks-Skiba, K., White, H., and Cooke, R. (1993) *J. Biol. Chem. 268*, 10046−10053.
18. Dantzig, J. A., Walker, J. W., Trentham, D. R., and Goldman, Y. E. (1988) *Proc. Natl. Acad. Sci. U.S.A. 85*, 6716−6720.
19. Margossian, S. S., and Lowey, S. (1982) *Methods Enzymol. 85*, 55−71.
20. Millar, N. C., and Geeves, M. A. (1988) *Biochem. J. 249*, 735−743.
21. Goodno, C. C. (1982) *Methods Enzymol. 85*, 116−123.
22. Kodama, T., Fukui, K., and Kometani, K. (1986) *J. Biochem. (Tokyo) 99*, 1465−1472.
23. Imamura, K., Tada, M., and Tonomura, Y. (1966) *J. Biochem. (Tokyo) 59*, 280−289.
24. Goodno, C. C. (1979) *Proc. Natl. Acad. Sci. U.S.A. 76*, 2620−2624.
25. Eden, D., and Highsmith, S. (1997) *Biophys. J. 73*, 952−958.
26. Highsmith, S., and Eden, D. (1986) *Biochemistry 25*, 2237−2242.
27. Provencher, S. W. (1976) *J. Chem. Phys. 64*, 2772−2777.
28. White, H. D., Belknap, B., and Jiang, W. (1993) *J. Biol. Chem. 268*, 10039−10046.
29. Resetar, A. M., and Chalovich, J. M. (1995) *Biochemistry 34*, 16039−16045.
30. Goody, R. S., and Mannherz, H. G. (1975) in *Protein−Ligand Interactions* (Sund, H., and Blauer, G., Eds.) pp 109−127, de Gruyter, Berlin.
31. Werber, M. M., Szent-Gyorgyi, A. G., and Fasman, G. D. (1972) *Biochemistry 11*, 2872−2883.
32. Kirshenbaum, K., Papp, S., and Highsmith, S. (1993) *Biophys. J. 65*, 1121−1129.
33. Bagshaw, C. R., and Trentham, D. R. (1974) *Biochem. J. 141*, 331−349.
34. Eccleston, J. F., and Trentham, D. R. (1979) *Biochemistry 18*, 2896−2904.

35. Bobkov, A. A., and Levitsky, D. I. (1995) *Biochemistry 34*, 9708−9713.
36. Moschcovich, L., Peyser, Y. M., Salomon, C., Burghardt, T. P., and Muhlrad, A. (1998) *Biochemistry 37*, 15137−15143.
37. Polosukhina, K., Eden, D., Chinn, M., and Highsmith, S. (2000) *Biophys. J. 78*, 1474−1481.
38. Johnson, W. C., Bivin, D. B., Ue, K., and Morales, M. F. (1991) *Proc. Natl. Acad. Sci. U.S.A. 88*, 9748−9750.
39. Hiratsuka, T. (1992) *J. Biol. Chem. 267*, 14949−14954.
40. Rayment, I., Smith, C., and Yount, R. G. (1996) *Annu. Rev. Physiol. 58*, 671−702.
41. Park, S. Ajtai, K., and Burghardt, T. P. (1996) *Biophys. Chem. 63*, 67−80.

BI001146D